

Kondo physics of magnetic adatoms on metallic surfaces when the onset of the surface conduction density of states crosses the Fermi level

J. Fernández¹ and P. Roura-Bas¹

¹*Centro Atómico Bariloche, CNEA, 8400 S. C. de Bariloche, Argentina*

We study the role of the onset of Shockley states, D_s , belonging to (111) surfaces of Cu, Ag and Au in the Kondo effect when a magnetic impurity is deposited on them. When D_s approaches to the Fermi level, E_F , thing that can be done by compressing (stretching) the metallic sample, we found that most of the thermodynamic and dynamic properties of the impurity are affected in a non trivial way. We model the system by a generic Anderson impurity model and solve it by using the numerical renormalization group, NRG, technique. In particular, the impurity contribution to magnetic susceptibility and entropy as a function of temperature exhibit negative values and goes to zero slowly in a logarithmic shape. Furthermore, we found a suppression of the spectral density weight at the Fermi level when $D_s \sim E_F$ even in the Kondo regime. As a consequence, the conductance through the impurity is strongly reduced by near 25% of the unitary value $2e^2/h$. Finally, we analyze these features in realistic systems like Co on Ag(111) reported in the literature.

PACS numbers: 72.15.Qm, 73.22.-f, 68.37.Ef

I. INTRODUCTION

In solid state physics, Shockley states arise when solving the Schrödinger equation in the context of nearly free electron models as a consequence of crystal termination. They are a common feature of (111) surfaces of noble metals.¹ In case of Ag, Cu and Au metals, the d-surface bands are well below the Fermi energy E_F , while the sp-surface ones are located around E_F .²

The nearly constant surface density of states (sDOS) abruptly starts below E_F at $D_s - E_F \approx -450$ meV for Cu,³ $D_s - E_F \approx -475$ meV for Au,⁴ and $D_s - E_F \approx -67$ meV for Ag.⁵ From scanning tunneling microscope (STM) measurements, the corresponding steps have been observed.⁴⁻⁶ Interestingly, the occupation of these surface states depends appreciably on particular variables such as temperature and the presence of adsorbed species, and more importantly by stretching the sample. Decreasing temperature, the onset of Ag(111) sDOS moves monotonically towards E_F .⁷ Stretching the Ag layers, induced by the film growth, shifts D_s up in energy, even beyond the Fermi level.⁸ Furthermore, the onset of sDOS can be changed by alloying the different noble metals at the surface.^{4,9} In addition, the construction of a piezoelectric-based apparatus for applying continuously tunable compressive and tensile strains to test samples is reported in Ref. 10. It can be used within a wide temperature range, including cryogenic ones.^{10,11} In particular, such a device can be used for moving D_s continuously across E_F .

On the other hand, the above mentioned metal surfaces are often used to host magnetic impurities (see figure 1). Several experiments were made to study atomic impurities (such as Co or Mn) over such surfaces.^{3,5,12-18} Moreover, complex magnetic molecules were also deposited on Ag, Cu and Au surfaces like FePc^{19,20} among others. With help of low-temperature STM measurements, in these systems the Kondo effect have been studied.

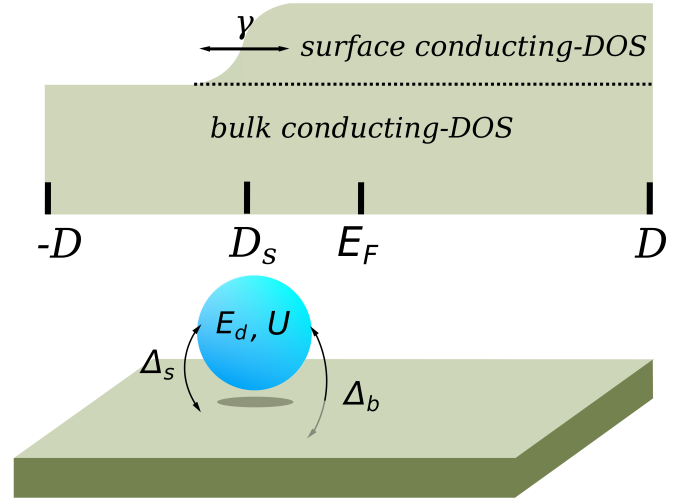


FIG. 1: Sketch of the setup. A magnetic impurity modeled as a single quantum dot with an energy level E_d and Coulomb repulsion U is deposited on the surface of a metal. The bulk density of the states extends from $-D$ to D while the surface contribution abruptly starts at D_s . Both systems are coupled via the hybridization parameters Δ_b and Δ_s . E_F indicates the Fermi energy.

In such measurements, the Kondo phenomena emerges through a narrow Fano-Kondo antiresonance in the differential conductance $G(V) = dI/dV$, where I is the current and V the applied voltage.

The width of $G(V)$ is usually related with the Kondo temperature, T_K , and below it the magnetic moment of the impurity is screened by the conduction electrons.²¹

The Kondo effect has the quality of universality in the sense that most of impurity properties display an universal shape once they are scaled by T_K . This fact makes T_K the only relevant energy scale of the problem and its precise estimation is always desirable.

Having mentioned that the onset of (111) surfaces can be move towards the Fermi energy and taking into account that the Kondo effect is a low energy phenomena, the question of how it is affected when $|D_s - E_F| \sim T_K$ raises. Interestingly, when $|D_s - E_F| \gg T_K$ the Kondo temperature as a function of D_s was found to display a power law $T_K \simeq C|D_s - E_F|^\alpha$.²²

In this paper we analyze the Kondo physics of a magnetic impurity on metallic surfaces when the onset of the surface conduction density of states crosses the Fermi level. We found that T_K loses the power law dependence and more importantly, both thermodynamic and transport properties of the impurity in the Kondo regime are strongly modified in a non trivial way.

Modeling the system with an Anderson impurity Hamiltonian, we employ the numerical renormalization group (NRG) technique as implemented in the NRG LJUBLJANA open source code²³.

In particular, when $|D_s - E_F| \leq T_K$ we found unusual temperature dependencies in the impurity properties like negative values of entropy, $S_{imp}(T)$, and magnetic susceptibility, $\chi_{imp}(T)$. Furthermore, since D_s can be moved towards E_F , we also analyze the conductance, $G(T)$, through the impurity encountering a strong suppression of the conductance at low temperatures when the onset approaches to E_F . Finally and making contact with experiments, we study the conductance within the regime in which measurements by Limot *et al.* in Ref.⁵ and by Moro-Lagares *et al.* in Ref.¹⁶ were made.

Our results are important in order to predict deviations of the Kondo properties from its usual behaviors in systems where the onset of sDOS moves towards the Fermi energy.

The paper is organized as follows. In Section II we described the theoretical model under study. Numerical results and its analysis are given in Section III. Finally, a summary and conclusions are presented in Section IV.

II. MODEL

The theoretical model we analyze in this paper, corresponding to the setup in figure 1, is defined by the following Hamiltonian

$$H = \sum_{k\sigma} \varepsilon_k^s s_{k\sigma}^\dagger s_{k\sigma} + \sum_{k\sigma} \varepsilon_k^b b_{k\sigma}^\dagger b_{k\sigma} + E_d \sum_{\sigma} n_{d\sigma} + U \sum_{\sigma} d_{\uparrow}^\dagger d_{\uparrow} d_{\downarrow}^\dagger d_{\downarrow} + \sum_{k\sigma} V_k^s [d_{\sigma}^\dagger s_{k\sigma} + \text{H.c.}] + \sum_{k\sigma} V_k^b [d_{\sigma}^\dagger b_{k\sigma} + \text{H.c.}] \quad (1)$$

where the first two terms correspond to surface and bulk non-interacting conduction electrons respectively. The operator d_{σ}^\dagger creates an electron with spin σ at the magnetic impurity with $n_{d\sigma} = d_{\sigma}^\dagger d_{\sigma}$. E_d and U are the energy level and Coulomb repulsion respectively. The

last two terms describe the hybridization between the impurity and conduction electrons.

As usual, we describe the bulk contribution to conduction electrons with a constant density of states, ρ_b , extended in a band-width from $-D$ to D . On the other hand, we model the surface contribution to the density of states including lifetime effects coming from quasiparticles interactions by a rounded-step function (see figure 1)

$$\rho_s(\omega) = \frac{\rho_s}{\pi} \left[\frac{\pi}{2} + \arctan((\omega - D_s)/(\gamma/2)) \right] \theta(D - |\omega|). \quad (2)$$

that starts at D_s and is extended to D where γ represents the inverse lifetime of the surface states.^{5,24,25} Regarding the upper limit of sDOS, it was found to be of the order of 1 eV in Au(111)² and 0.2 eV in Ag(111)⁶. In any case, we chose for simplicity the upper limit to coincide with the one of the bulk DOS, D . This choice is justified because it does not modified the low energy properties, near the Fermi level, which is the central point in our work. To provide an order of magnitude of ρ_b and ρ_s , they were found to be 0.135/eV and 0.0466/eV in case of Ag(111) respectively.¹⁷

The effect of the conduction bands on the impurity can be put in terms of an energy dependent hybridization within the range $-D$ to D

$$\begin{aligned} \Delta(\omega) &\equiv \pi \sum_{\nu k \sigma} |V_k^\nu|^2 \delta(\omega - \varepsilon_k^\nu) \\ &= \Delta_s \tilde{\rho}_s(\omega) + \Delta_b. \end{aligned} \quad (3)$$

where $\Delta_\nu = \pi |V^\nu|^2 \rho_\nu$ and $\tilde{\rho}_\nu = \rho_\nu(\omega)/\rho_\nu$ is the bare density of states of the band electrons, normalized to its constant value.

The retarded Green function of the impurity is given by

$$G_{d\sigma}(z) = \frac{1}{z - E_d - \Sigma_{\Delta\sigma}(z) - \Sigma_{U\sigma}(z)}, \quad (4)$$

where $z = \omega + i0$ and $\Sigma_{U\sigma}(z)$ and $\Sigma_{\Delta\sigma}(z)$ are the interacting (due to the Coulomb repulsion U) and the non-interacting (due to the one body hybridization $\Delta(\omega)$) contributions to the self-energy respectively.

The non-interacting part of the self-energy is defined by the hybridization function

$$\Sigma_{\Delta\sigma}(\omega) = \Gamma(\omega) - i\Delta(\omega), \quad (5)$$

where the real part $\Gamma(\omega)$ can be obtained from $\Delta(\omega)$ by means of a Kramers-Kronig transformation.

As we mentioned in the Introduction, we solve the Hamiltonian in Eq. (1) by using the NRG technique. In addition to the usual z -averaging²⁶ and sigma-trick²⁷ refinements when calculating thermodynamics and dynamical properties, the NRG-ljubljana uses an improved

discretization scheme²⁸ that allows NRG method to handle with energy dependent hybridizations²⁵. As usual, the half bandwidth of the bulk conduction electrons is taken as the unit of energy, $D = 1$ and the Fermi energy is chosen to be $E_F = 0$. Furthermore, we have used a renormalization parameter $\Lambda = 2$ and a number of different values of z , $N_z = 16$, in all NRG calculations.

III. RESULTS

A. Sharp-step surface DOS

We start this section considering that the surface density of states can be modeled by a step function, that is without the broadening introduced by the inverse lifetime, $\gamma = 0$. This case was considered before for a fixed value of $|D_s| \gg T_K$.^{16,17,22,25,29} As we will show in this work, in the regime $|D_s| \ll T_K$ the step shape of sDOS contains the key ingredients related with the role of the onset in the Kondo physics.

1. Kondo temperature as a function of D_s

It will be instructive to present a brief summary of the main results of Ref. 22 regarding the variation of T_K with D_s for $|D_s| \gg T_K$. When the onset of the surface contribution to conduction density of states is near the Fermi energy, the Kondo temperature as a function of D_s was found to display a power law $T_K \simeq C|D_s|^\alpha$, where the exponent α depends on the relative intensities between surface and bulk hybridizations with the impurity, Δ_s/Δ_b , and the ratio between on-site and Coulomb energies E_d/U as well as the sign of D_s and C encloses the other dependences. This power law was obtained from a poor man's scaling (PMS)^{30,31} approach to the effective Kondo model and confirmed numerically by using the Non-Crossing Approximation (NCA)^{30,32}. The validity of the above dependence applies for small values of $|D_s| \ll D$ but they are limited to $|D_s| \gg T_K$. Unfortunately, neither PMS nor NCA can describe the regime $|D_s| \leq T_K$. In case of PMS, the renormalization group procedure ceases to be valid³⁰ while in case of NCA, there are inaccurate results when dealing with small energies as compared with the Kondo one³².

Specifically, the Kondo scale was found to depend on the onset D_s in the following way

$$T_K \simeq A|D_s|^\eta D^{1-\eta} \exp \left[\frac{\pi E_d(E_d + U)}{2U(\Delta_b + \Delta_s)} \right],$$

$$\eta = \frac{\Delta_s}{(\Delta_b + \Delta_s)} \left(1 + \frac{E_d}{U} \right), \text{ for } D_s < 0, \quad (6)$$

and

$$T_K \simeq B(D_s)^\zeta D^{1-\zeta} \exp \left[\frac{\pi E_d(E_d + U)}{2U\Delta_b} \right],$$

$$\zeta = \frac{\Delta_s E_d}{\Delta_b U}, \text{ for } D_s > 0. \quad (7)$$

Both equations are valid in the limit of $|D_s| \gg T_K$ and when charge fluctuations are limited only to two configurations, $0 \leq n_d \leq 1$ for $E_d < \infty$, $U \rightarrow \infty$ and $1 \leq n_d \leq 2$ for $E_d + U < \infty$, $\{E_d, -U\} \rightarrow -\infty$. The exponents η and ζ were confirmed by NCA calculations for several values of the ratio Δ_s/Δ_b .

Within our NRG calculations, we get the Kondo temperature from the thermodynamic properties of the Hamiltonian according to Wilson's definition, $k_B T_K \chi_{imp}(k_B T_K)/(g\mu_B)^2 = 0.07$, being $\chi_{imp}(k_B T)$ the impurity contribution to the magnetic susceptibility as a function of temperature³³. Through the rest of the manuscript we set $g\mu_B = 1$ and $k_B = 1$.

In figure 2 we show the results for T_K as a function of D_s in the selected case of $\Delta_s = \Delta_b$. The top panel displays the case of having $U \rightarrow \infty$. From Eq. (6), a value of $\eta = 1/2$ is expected. Fitting the NRG results with a power law of the form $A|D_s|^\eta$ for negative values of D_s we obtain an exponent $\eta = 0.49$. On the other hand, the lower panel shows the results in case of $E_d + U < \infty$ while $\{E_d, -U\} \rightarrow -\infty$ for which an exponent $\zeta = -1$ for positive values of D_s is expected. We obtain $\zeta = -0.94$ from the fitting. In both cases the accuracy of the fittings is confirmed by a correlation coefficients (cc) near to unity with an error of 10^{-4} . The present results, also limited to $T_K \ll |D_s|$, verifying the corresponding ones presented in Ref. 22. Furthermore, other ratios of Δ_s/Δ_b (not shown) were studied and also agree with the PMS and NCA results.

As we mentioned, the range $T_K \geq |D_s|$ is not accessible neither by PMS nor NCA. In figure 3 we show the values of T_K when D_s approaches to the Fermi energy from negative values in case of $U \rightarrow \infty$ and finite on-site energy E_d .

We can see from the plot that the scaling law in Eq. (6) breaks down as soon as $-D_s$ approaches to T_K . Furthermore, T_K seems to be constant in the range $|D_s| \ll T_K$ and saturates at a value T^* when $D_s = 0$ (dashed line). The corresponding values for positive D_s , although they do not obey any scaling, are present in order to show that a continuity function $T_K(D_s)$ is obtained when D_s crosses the Fermi energy. Finally, we found (not shown) a similar deviation of the power law in case of Eq. (7).

2. Thermodynamic properties in the range $|D_s| \ll T_K$

In what follows we turn our attention to the analysis of the Kondo physics through the impurity contribution to thermodynamic properties in the range $|D_s| \ll T_K$ and in particular for $D_s = 0$.

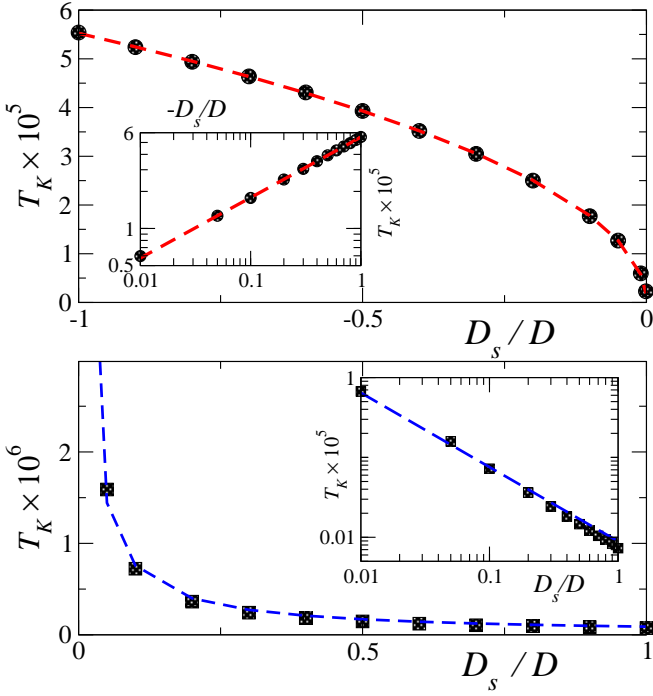


FIG. 2: (Color online) Kondo temperature as a function of D_s for $E_d = -0.04D$, $U \rightarrow \infty$ (top panel) and $E_d + U = 0.04D$, $\{E_d, -U\} \rightarrow -\infty$ (bottom panel). In both cases $\Delta_b = \Delta_s = 0.5D$. Similar values of E_d and $E_d + U$ were used in Ref. 22. Fitting parameters: $A = 5.52 \times 10^{-5}$, $\eta = 0.49$, $cc = 0.9999$, $B = 8.9 \times 10^{-8}$, $\zeta = -0.94$, $cc = 0.9998$. The insets show the results in a logarithmic scale.

Interestingly, when $|D_s| < T_K$, the impurity magnetic susceptibility times temperature, $T\chi_{imp}(T)$, approaches to zero from negative values and very slowly. This unusual low-temperature behavior is shown in figure 4 for the same set of model parameters that figure 3. Notice that for finite values of D_s , the magnitude of $T\chi_{imp}(T)$ vanishes at sufficient low temperature. In particular, for $D_s = 0$, $T\chi_{imp}(T)$ approaches to zero in the limit of $T \rightarrow 0$. From the results of figure 3, we do not expect a significant variation of the impurity properties for $D_s > 0$.

When analyzing thermodynamic properties of the impurity, we also notice that similar low temperature features also appears in the impurity contribution to the entropy, $S_{imp}(T)$. That is, $S_{imp}(T)$ goes to zero at low temperature from negative values (see top panel of figure 6).

We remain the reader that the impurity contribution to $\chi(T)$ and $S(T)$ are given by $\chi_{imp}(T) = \chi_{tot}(T) - \chi_{tot}^{(0)}(T)$ and $S_{imp}(T) = S_{tot}(T) - S_{tot}^{(0)}(T)$ where $\chi_{tot}^{(0)}(T)$ ($S_{tot}^{(0)}(T)$) denotes the system without impurity.^{33,34} Therefore, even when $\chi_{tot}(T)$ ($S_{tot}(T)$) and $\chi_{tot}^{(0)}(T)$ ($S_{tot}^{(0)}(T)$) are separately positive, the impurity contribution can be negative.

One may wonder if the Coulomb repulsion takes any

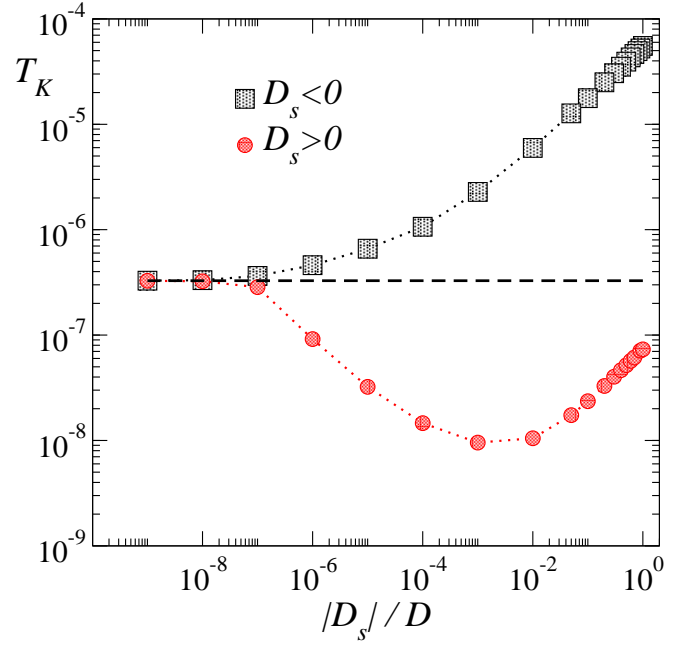


FIG. 3: (Color online) Kondo temperature as a function of D_s for the same set of model parameters that in top panel of figure 2. Dashed line stands for $D_s = 0$ representing an energy scale $T^* = 3.3 \times 10^{-7} D$.

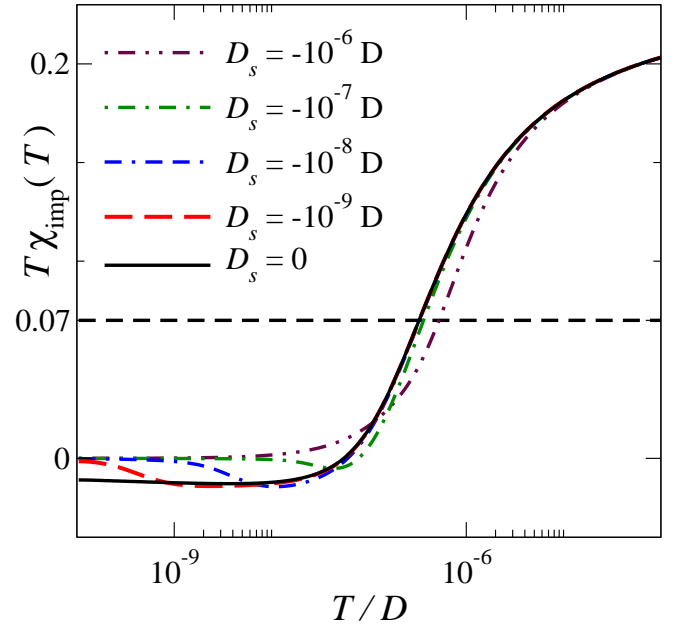


FIG. 4: (Color online) Impurity magnetic susceptibility as a function of temperature for the same set of model parameters that in figure 3 and for different values of D_s/D . Black dashed constant line indicates the criteria for defining the Kondo temperature.

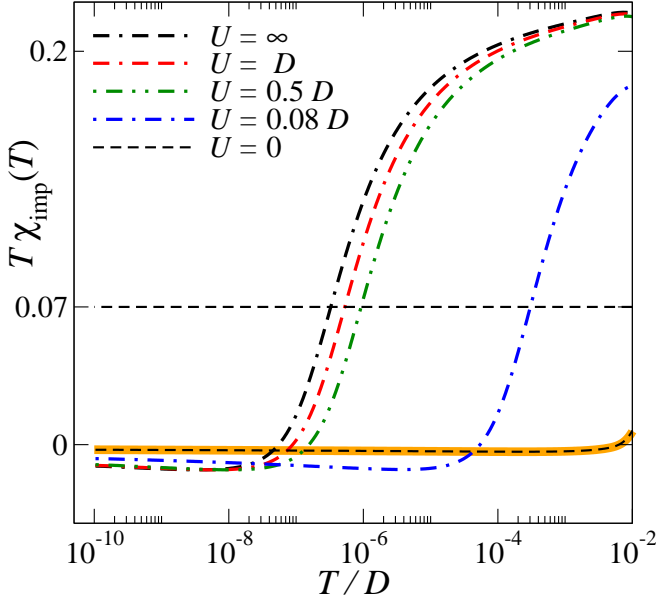


FIG. 5: (Color online) Impurity magnetic susceptibility as a function of temperature in case of $D_s = 0$ and for different values of the Coulomb repulsion U and for $E_d = -0.04D$. Solid orange line corresponds to the analytic result for $U = 0$ according to Eq. (8).

role in this behavior. In figure 5 we fix the onset of the surface density of states in $D_s = 0$ and $E_d = -0.04D$ and analyze $\chi_{imp}(T)$ for several values of U from the non-interacting case $U = 0$ to $U \rightarrow \infty$.

In fact, they are already present for the non-interacting case $U = 0$. The distinctive feature of the model Hamiltonian in Eq. (1) is enclosed in the one-body self-energy in Eq. (5), so in the following we analyze the magnetic susceptibility and entropy for the non-interacting model.

The impurity magnetic susceptibility and entropy for the non-interacting version of the Hamiltonian in Eq. (1) are given by the following expressions

$$S_{imp}(T) = \frac{2}{\pi T} \text{Im} \int_{-\infty}^{+\infty} d\omega f'(\omega) \omega \ln G_{0d}^{-1}(\omega) \quad (8)$$

$$T\chi_{imp}(T) = \frac{1}{2\pi} \text{Im} \int_{-\infty}^{+\infty} d\omega f'(\omega) (1 - 2f(\omega)) \ln G_{0d}^{-1}(\omega),$$

where $G_{0d}^{-1}(\omega) = \omega - E_d - \Sigma_{\Delta}(\omega)$ is the non-interacting electron impurity Green function independently of the spin.

Both magnitudes were calculated in the case of $D_s = 0$ and its results as a function of temperature are displayed in figure 6 represented by solid lines. Clearly, the same features that in figures 4 and 5 are present. Although it is not necessary, we take the opportunity to benchmark the NRG when calculating the same thermodynamic impurity contribution for $U = 0$. As it is clear from the figure, the results obtained are on-top of the analytical

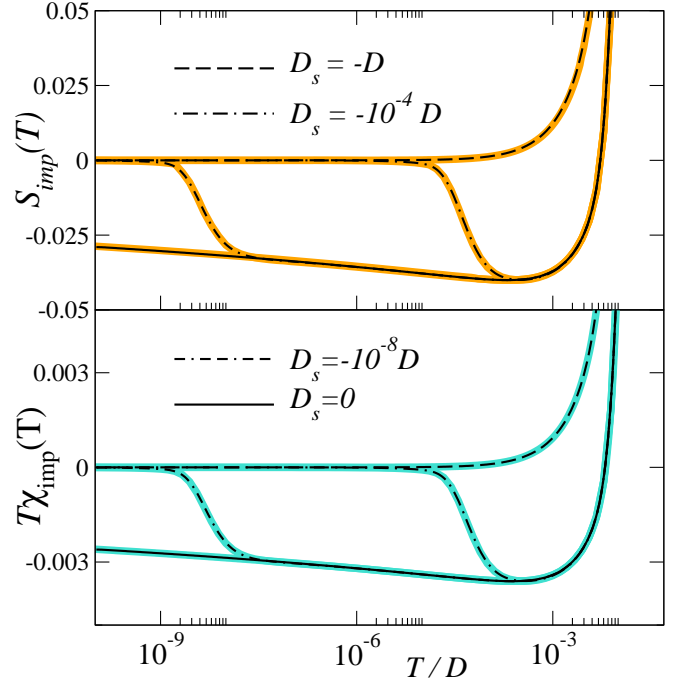


FIG. 6: (Color online) In thick lines, $S_{imp}(T)$ (top panel) and $T\chi_{imp}(T)$ (bottom panel) results for $D_s = U = 0$ from Eqs. 8. Black light lines correspond to NRG calculations.

ones. This accuracy when dealing with energy dependent hybridizations is due to the improved discretization scheme detailed in Ref.²⁸.

The low-temperature behavior of Eq. (8) is given by the corresponding low-energy form of the one-body self-energy, which in the limit of $D_s = 0$ is

$$\Sigma_{\Delta}(\omega) \sim \frac{\Delta_s}{\pi} \ln \left| \frac{\omega}{D} \right| - i\Delta(\omega). \quad (9)$$

Note the divergent form at low energies. Then, the impurity entropy and magnetic susceptibility becomes

$$S_{imp}(T) \sim -\frac{(1/2)\ln 4}{\ln(1/2T)} + O(T^2)$$

$$T\chi_{imp}(T) \sim -\frac{(1/8)}{\ln(1/2T)} + O(T^2). \quad (10)$$

Remarkably, the usual Fermi liquid properties for $|D_s| \leq T_K$ are recovered at low enough temperature and for the special case in which the onset of the surface DOS coincides with the Fermi energy, they are reached logarithmically slowly.

Here we would like to mention the work of Mitchell and Fritz, Ref. 35, in which they analyze the Kondo effect in graphene with vacancies. In spite of being very different systems, the one studied by Mitchell and co-workers and the present one, they also found negative

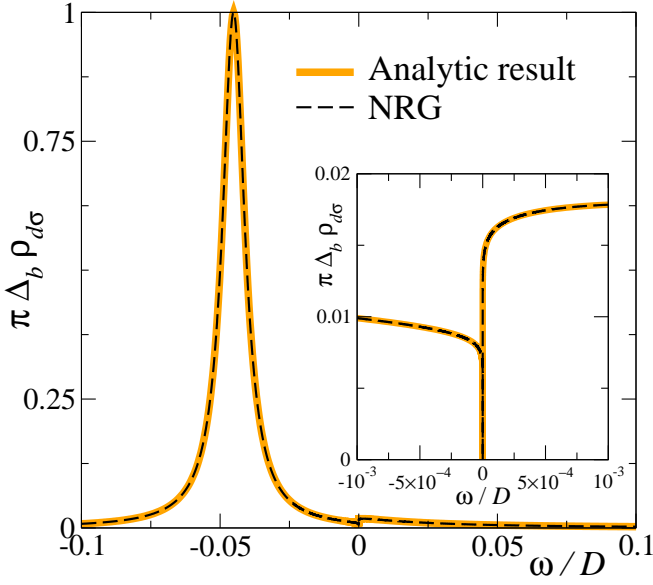


FIG. 7: (Color online) Non-interacting impurity spectral density $\rho_{0d}(\omega)$ for $D_s = 0$ obtained from Eq. (4) with $\Sigma_{U\sigma}(z) = 0$ and NRG with $U = 0$. Other parameters as in figure 2.

impurity contributions to magnetic susceptibility and entropy at low temperatures independently of the value of the Coulomb repulsion. In that case, the responsible of such behavior is attributed to a logarithmically divergent *imaginary* part of the one-body hybridization Σ_Δ coming from a zero mode in graphene with defects. In our case, we have a logarithmically divergent *real* part of the one-body hybridization coming from a non-analyticity in the conduction DOS. In any case, both hybridization shapes give rise similar low-temperature features in the impurity properties.

3. Spectral density for $D_s = 0$

Since $\Sigma_\Delta(\omega)$ becomes infinite for $D_s = \omega = 0$, it is expected that the impurity spectral density, $\rho_{0d}(\omega) = -\text{Im}G_{0d}(\omega)/\pi$, vanishes at the Fermi energy. This is explicitly shown in figure 7 in which both, the analytical and NRG calculations are again on-top one each other.

As we have shown, the Coulomb repulsion is not responsible for this effect so one may wonder in which way this logarithmic energy dependence affects the Kondo effect. Once the interaction U is turned on and the temperature is lowered, the spectral weight at the Fermi level should be increased due to the appearance of the Kondo peak.³⁰ Therefore, a competition between both effects is expected. In figure 8 the spectral density is shown for two selected values of the Coulomb repulsion, $U = -2E_d$ and $U = \infty$ and for $D_s = 0$. The NRG calculations were done at $T = 10^{-3}T_K$ being T_K the corresponding one for each value of U accordingly to figure 5. Several aspects

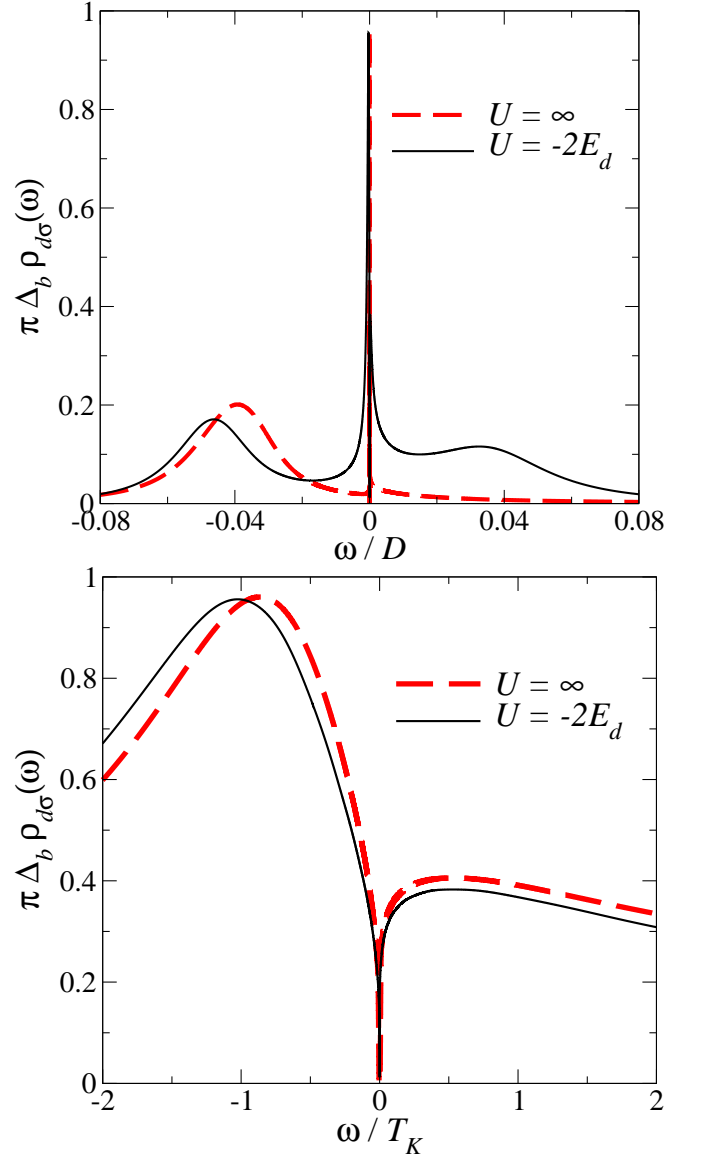


FIG. 8: (Color online) Top panel: spectral densities $\rho_{d\sigma}$ as a function of frequency for $D_s = 0$ and $U = -2E_d$ (solid line) and $U = \infty$ (dashed line). $E_d = -0.04$ and $\Delta_s = \Delta_b = 0.005$. Lower panel: low energy region in units of ω/T_K being $T_K(U = -2E_d) = 3.04 \times 10^{-4}D$ and $T_K(U = \infty) = 3.40 \times 10^{-7}D$. Calculations were done at $T = 10^{-3}T_K$.

can be discuss from these results. In a first place, the top panel shows the spectral density in its extended frequency region. The solid line has a value of the Coulomb interaction in such a way that $2E_d + U = 0$, which is the usual condition for particle-hole symmetry. This symmetry is clearly broken due to the asymmetry in the hybridization function in Eq. (3) (see also the cartoon of the conduction DOS in figure 1). While the lower charge transfer peak, locate at energy $\omega \sim E_d$ has a width of the order of $4\Delta_b$,^{36,37} the upper one, locate at $\omega \sim E_d + U$ has a width of the order of $4(\Delta_b + \Delta_s)$ and, as consequence, its

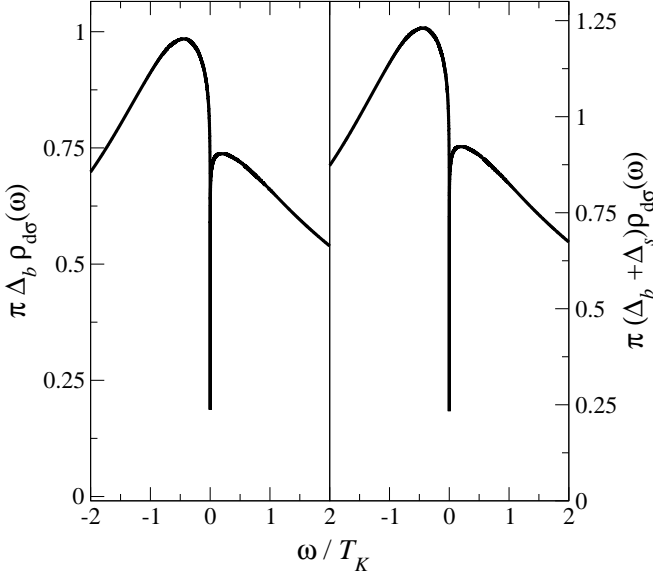


FIG. 9: (Color online) Spectral density $\rho_{d\sigma}$ in the low energy region in units of ω/T_K ($T_K = 3 \times 10^{-5}D$) for $D_s = 0$ and $\Delta_s = 0.25\Delta_b = 0.00125$. $U = -2E_d$ with $E_d = -0.04$. Left panel: $\rho_{d\sigma}$ scaled by $\pi\Delta_b$. Right panel: $\rho_{d\sigma}$ scaled by $\pi(\Delta_b + \Delta_s)$.

intensity is reduced. In the $U = \infty$ case, a similar width of $4\Delta_b$ in the unique charge transfer peak is shared. The central peak correspond to the Kondo resonance. In a similar manner that the width of the Fano-Kondo antiresonance is related with T_K , the width of the Kondo peak does. In relation with the low energies features of the spectral density, the bottom panel of figure 8 shows a detail of the Kondo resonance. Once the energy dependence in both curves is shown in units of T_K , they are quite similar as a consequence of the universality of the Kondo phenomena.

The logarithmically divergence of the one-body hybridization splits the Kondo resonance into two pieces around the Fermi level. Furthermore, a suppression of the spectral weight at $\omega = E_F$ is observed independently of the value of the Coulomb repulsion. Note that for negative energies closes to the Fermi one, the Kondo peak seems to agree with the usual Friedel sum rule $\rho_{d\sigma}(0) = 1/\pi\Delta$, with $\Delta = \Delta_b$. On the other hand, since the sDOS is already turned on for positive energies, the hole contribution of the Kondo resonance, $\omega \gtrsim 0$, seems to be related with the total contribution $\Delta = \Delta_b + \Delta_s$. We have confirmed the last statement by plotting the spectral density for another relation between Δ_b and Δ_s . In particular we choose the ratio $\Delta_s/\Delta_b = 1/4$ which has found to be the lower limit for the surface contribution to the total hybridization in Co impurities deposited on Ag(111) surface.¹⁶ What we observed from the plot is that while the negative portion of the Kondo resonance approaches to one when scaled by $\pi\Delta_b$, the positive one reaches the same value but when it is scaled

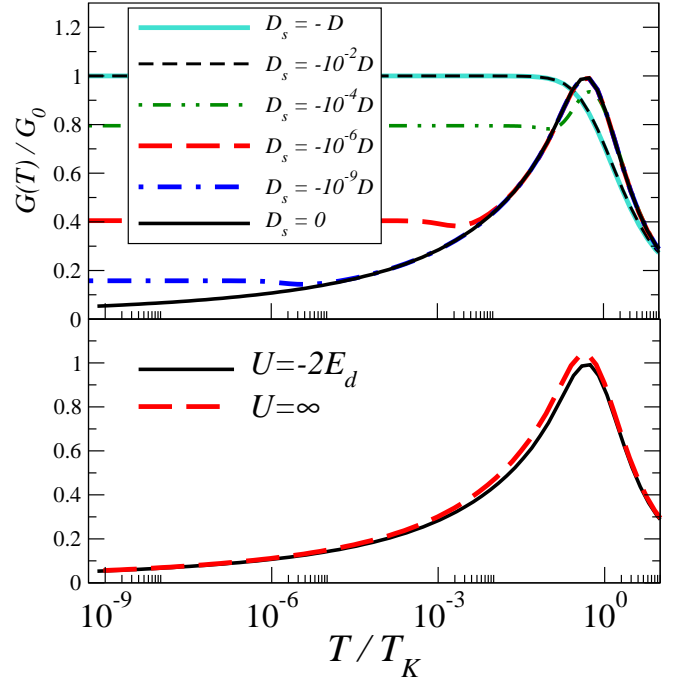


FIG. 10: (Color online) Equilibrium conductance in units of $G_0 = 2e^2/h$ as a function of temperature in units of T_K . Top panel: Several values of D_s for the case $U + 2E_d = 0$ with $U = 0.08D$. Bottom panel: $D_s = 0$ for the cases $U + 2E_d = 0$ with $U = 0.08D$, black solid curve, and $U \rightarrow \infty$, red dashed line.

by $\pi(\Delta_b + \Delta_s)$. Note that for the selected parameters the Kondo resonance is slightly asymmetric with more weight in the negative region, so it is closer to one for negative energies than for the positive ones.

In any case, the usual Friedel sum rule does not apply since $\rho_{d\sigma}(0) \sim 0$. Instead, as we will see, the weight of the spectral density at the Fermi energy is consistent with the generalized Friedel sum rule.^{38,39}

4. Conductance through the impurity and occupation

The reduction of the spectral weight at low energies affects the transport properties of the model.

The equilibrium conductance $G(T)$ directly depends on $\rho_{d\sigma}(\omega)$ ⁴⁰

$$G(T) = G_0 \frac{\pi}{2} \sum_{\sigma} \int_{-\infty}^{+\infty} d\omega [-f'(\omega)] \Delta(\omega) \rho_{d\sigma}(\omega), \quad (11)$$

where $G_0 = 2e^2/h$ is the quantum of conductance. In particular, a strong reduction of the equilibrium conductance, $G(T)$, at low temperatures is expected. In figure 10 we show the NRG calculations for the conductance as a function of temperature. In the top panel we have fixed $U + 2E_d = 0$ with $U = 0.08D$ while varying the values

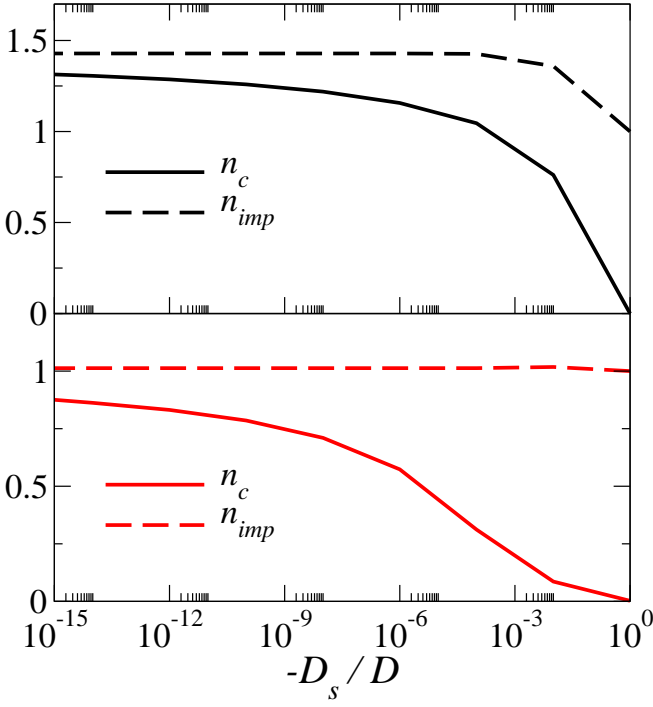


FIG. 11: (Color online) n_c and n_{imp} as a function of D_s for $U + 2E_d = 0$. Top panel: $U = 0$. Bottom panel: $U = 0.08D$. In both cases we have used $\Delta_s = \Delta_b = 0.005D$.

of the onset D_s . When $D_s = -D$ the surface contribution to the hybridization agrees with the bulk one and the conductance displays the usual behavior reaching the maximum value for this problem of G_0 for temperatures $T \ll T_K$. For smaller values of $|D_s|$ but still large as compared with the corresponding T_K , the shape of the conductance is not affected. However, when $-D_s$ is of the order of T_K ($\sim 10^{-4}D$), $G(T)$ saturates at a reduced fraction of G_0 . The reduction of the saturated conductance grows as D_s approaches to zero. In the limiting case of $D_s = 0$, the conductance vanishes at low temperatures in a logarithmic shape.

In the bottom panel of figure 10 we show the obtained values of $G(T)$ for $D_s = 0$ and two different values of the Coulomb repulsion, $U + 2E_d = 0$ with $U = 0.08D$, black solid curve, and $U \rightarrow \infty$, red dashed line. As it is clear from the results, when scaling the temperatures by the corresponding Kondo one, both curves display an identical temperature dependence as expected from the universality of the Kondo effect.

The results of the intermediate plateaus in the conductance can be understood in terms of the generalized Friedel sum rule.^{38,39}

$$\begin{aligned} G(T)/G_0 &= \sin^2\left(\frac{\pi}{2}(n_{imp} - n_c)\right) \\ &= \pi(\Delta_b + \Delta_s)\rho_{d\sigma}(0), \end{aligned} \quad (12)$$

where n_{imp} is the impurity occupation and

$$n_c = -\text{Im} \sum_{\sigma} \int_{-\infty}^{E_F} \frac{d\omega}{\pi} G_{d\sigma}(\omega) \frac{\partial \Delta(\omega)}{\partial \omega}, \quad (13)$$

is related with the change of the charge in the conduction band as a consequence of the presence of the impurity. In the usual case of a flat hybridization, this term vanishes due to $\frac{\partial \Delta(\omega)}{\partial \omega} \sim 0$. However in our case we expect its influence to be rather large when $D_s \sim E_F$. For the non-interacting model, we evaluate Eq. (13) and together with the results of the impurity occupation, Eq. (12) can be verified. In the top panel of figure 11 we show the results of n_c and n_{imp} at zero temperature and as a function of D_s is the case of $U + 2E_d = 0$ with $U = 0$. While the impurity population is rather constant, it is clear that n_c approaches to n_{imp} as $|D_s|$ is decreased. Therefore, both $G(T \rightarrow 0)$ and $\rho_{d\sigma}(\omega \rightarrow 0)$ vanish when $D_s \rightarrow 0$. In the bottom panel of figure 11 we show the NRG results for n_c and n_{imp} at temperature $T = 10^{-3}T_K$ and as a function of D_s is case of $U + 2E_d = 0$ with $U = 0.08D$. As we have previously mentioned, particle-hole symmetry is slightly broken (see figure 8) and therefore the impurity occupation is very close, but not exactly, to one. However, n_c strongly changes from zero ($D_s = -D$) to one ($D_s = 0$). In this case, when interactions are turning on, we obtain n_c not directly from Eq. (13) but from the more accurate values of the low temperature conductance according to Eq. (12). Note that in the case of $D_s = 0$ the result $n_c = n_{imp}$ is only reached asymptotically for $T \rightarrow 0$, see figure 10.

B. rounded-step surface DOS

We ending the present work by considering finite lifetime effects, γ , leading to a smoother onset of the band edge as shown in Eq. (2).

This is specially important to make contact with real systems. In particular with the experiment of Limot and co-workers⁵ in which the authors perform scanning tunneling spectroscopy measurements of magnetic (Co) and non-magnetic (Ag) atoms on Ag(111) and Cu(111) and analyze a bound state that appears after impurity deposition near the onset of sDOS. In case of Co/Ag(111) and Co/Cu(111) a dip corresponding to a Fano-Kondo antiresonance appears at the Fermi level. For a quantitative analysis of the experiment, the authors model the surface DOS by including lifetime effects.

Therefore, it is interesting to see how rapidly the logarithmic shapes of the analyzed properties in this paper are blurring in the presence of γ . When a Co atom is deposited on a clean Ag(111) surface, the measure $T_K \sim 83K$ is found and the data is adjusted with $\gamma = 7meV = 81.2K$ and therefore $\gamma \sim T_K$. On the other hand, when a Co atom is deposited on Cu(111) the values were $T_K \sim 63K$ and $\gamma = 24meV = 278.4K$ which leads to a ratio $\gamma/T_K \sim 4.4$.

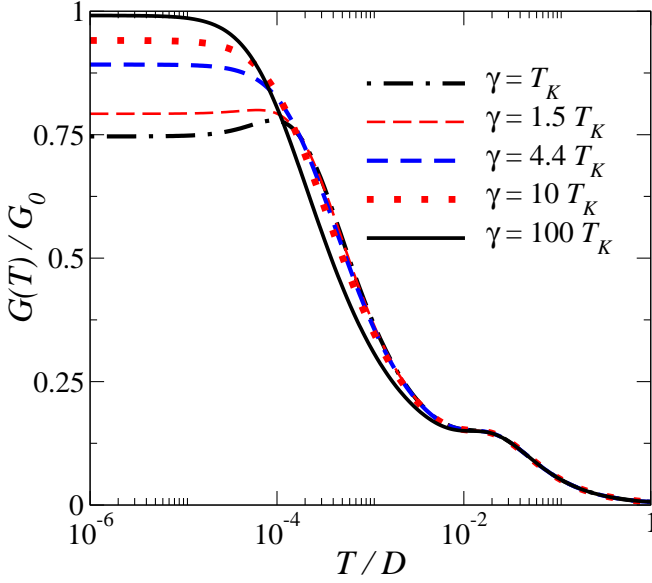


FIG. 12: Conductance as a function of temperature in case of $D_s = 0$ for several values of the inverse lifetime γ in units of T_K . As a reference, we use T_K corresponding to the black solid line in figure 8. $\gamma = T_K$ and $\gamma = 4.4T_K$ represent Co/Ag(111) and Co/Cu(111) respectively in Limot's experiment, while $\gamma = 1.5T_K$ represents Co/Ag(111) in Moro-Lagares' experiment.

In figure 12 we show the NRG results for the conductance as a function of temperature when the surface hybridization is given by Eq. (2) and for several values of the ratio γ/T_K . Here, we do not expect to make a quantitative description of each system mentioned above, but provide an analysis of what will be the effect of γ given the measure values of T_K . To this end, we have chosen a generic set of model parameters, E_d , U , Δ_b and Δ_s and compared the effect of γ against the obtained T_K . Provided that in the Kondo regime, the only relevant energy scale is in fact T_K and all magnitudes display a universal dependence when scaled by it, as for instance the spectral density in figure 8 (lower panel) or the conductance in figure 10, the results in figure 12 are quite general. The case of $\gamma/T_K = 1$ represents Co/Ag(111) in Limot's experiment. Clearly, when the onset of the surface states coincides with the Fermi energy, even in the case of having a lifetime in the DOS, the conductance is reduced significantly, near a factor 25% of the usual ideal value of G_0 . The case of $\gamma/T_K = 4.4$ represents Co/Cu(111) with also an important reduction of the low temperature conductance. For comparison, we also show the case $\gamma/T_K = 10$ for which the effect of the step is still present. Only when $\gamma/T_K \geq 100$ the conducting DOS is smooth enough to get $n_c \sim 0$ and the ideal conductance can be reached. Note however that here we are not including other degrees of freedom in the system that contribute to enlarge the inverse lifetime in sDOS. Such contributions should be included in order to fully analyze

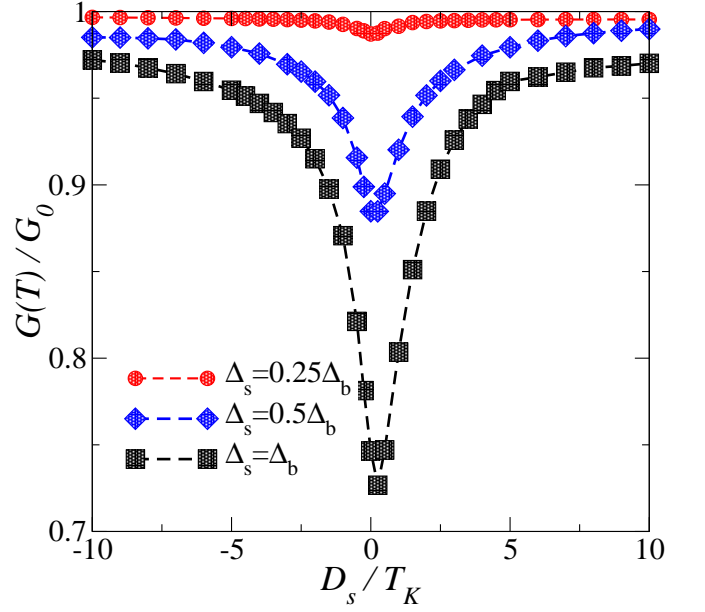


FIG. 13: Saturated conductance extracted from the low temperature plateaus in figure 12 as a function of D_s for several values of the ratio $r_{sb} = \Delta_s/\Delta_b$. $\gamma = T_K$ as Co/Ag(111) in Limot's experiment where T_K corresponding to the black solid line in figure 8.

the Kondo properties.

In addition to the Limot's experiment, the Moro-Lagares and co-workers one in Ref. 16, also study the Kondo phenomena that appears after deposition of a Co atom on a clean Ag(111) surface. In that work, the main result is a quantification of the role of the surface state in the Kondo effect and provides a lower bound for the ratio of hybridizations $r_{sb} = \Delta_s/\Delta_b = 1/4$.

Regarding T_K , the Fano-Kondo line shape is also analyzed and they found $T_K = 52K$ which increases the ratio $\gamma/T_K \sim 1.56$ as compared with Limot's work. The discrepancy between the Kondo temperature estimated by Limot *et al.* and Moro-Lagares *et al.* is explained in Ref. 41 and will not be discussed here. For this ratio between γ and T_K , the low temperature plateau in the conductance is reduced by near 20%.

In any case, the low temperature dependence of $G(T)$ is modified by the presence of the onset D_s even if a non vanishing inverse lifetime γ is incorporated when describing the surface conducting electrons.

Another way to observe the influence on transport measurements when moving the onset of sDOS, we plot in figure 13 the saturated conductance as a function of D_s . When $\gamma = T_K$, as Co/Ag(111) in Limot's experiment, a dip centered in $D_s = 0$ is clearly visible. The intensity of the dip depends on the ratio r_{sb} . Increasing r_{sb} results in an increment of the dip intensity. Once $|D_s| \gg T_K$, the conductance approaches towards G_0 independently of r_{sb} . Regarding the values of the ratio r_{sb} , R. Žitko in Ref. 25 arguments in favor of $r_{sb} = 1$ while the experiment

of Moro-Lagares, as we have mentioned, results in $r_{sb} \geq 1/4$. Note that from the results shown in figure 10, for $\gamma = 0$ the dip reaches its maximum intensity, $G(D_s = 0) \rightarrow 0$ independently of r_{sb} . Therefore, for the whole realistic values of r_{sb} , even if γ is present, evidence in the conductance through the impurity when D_s crosses the Fermi level should be present.

IV. SUMMARY

We have analyzed thermodynamic and dynamical properties of a magnetic ad-atom deposited on a metal surface which contains a rounded step in the surface contribution to the total density of states of conduction electrons. The model represents realistic setups for magnetic ad-atoms, like Co, on (111) surface of Cu, Ag and Au. In such metals, a two-dimensional surface band (Shockley states) starts at an energy D_s moderately below the Fermi level. As we mentioned in the Introduction, D_s can be move continuously.

Within this framework, we have studied the low temperature properties inside the Kondo regime as a function of D_s , in particular when it crosses E_F .

Firstly, we confirm by means of exact numerical renormalization group calculations, the power law Kondo temperature dependence on D_s found recently by using Poor man's scaling arguments and Non Crossing Approximation calculations in Ref. 22. After that, we focus on the physics that emerges from $D_s = 0$. We investigate several magnitude of interest, like impurity contribution to magnetic susceptibility and entropy, spectral density and equilibrium conductance. In all magnitudes, the step in surface DOS plays an important role when D_s approaches to E_F . Interestingly, the magnetic susceptibility and entropy as a function of temperature exhibit negative values and goes to zero slowly in a logarithmic shape. This re-

sults becomes independently of the impurity parameters such as the Coulomb repulsion being already present in the non-interacting case.

Secondly, we examine the impurity spectral density as well as the conductance. Both are larger affected by D_s . The results are interpreted in terms of the generalized Friedel sum rule in which the change of the charge in the conduction band, n_c , strongly depends on D_s .

Finally, we make emphasis in the relevance of our study not only for academic reasons but also in real experiments. We analyze the situation in the experiment made by Limot *et al.* in Ref. 5 and also in the one perform by Moro-Lagares and co-workers one in Ref. 16.

In both experiments a dip in the dI/dV representing the Fano-antiresonance is found at bias voltage $V = 0$. The dip is a clear manifestation of the Kondo resonance in the spectral density of Co. Although the results of figure 8 represent the limit case of $D_s \sim 0$, the shape and intensity of such dips are already affected by the step in the surface DOS even for finite values of D_s . In particular, we have found that, if D_s is moved towards E_F , measurable effects emerge. When the low-temperature conductance is plotted as a function of D_s , thing that can now be experimentally done¹⁰, we show that a dip should be present around $D_s \sim 0$. Therefore, we expect that our work stimulates further research on the area of magnetic ad-atom on metallic surfaces.

Acknowledgments

We thank A. A. Aligia and L. O. Manuel and I. Hamad for useful comments and careful reading of the manuscript. This work was sponsored by PIP 364 of CONICET (Argentina) and PICT xxx. 2013-1045 of the ANPCyT.

¹ *Impurity-induced localization of the 2D surface-state continuum on a metal surface*; J. P. Gauyacq, A. G. Borisov, and A. K. Kazansky, Appl. Phys. A **78**, 141 (2004).

² Harald Ibach; *Physics of Surfaces and Interfaces* (Springer-Verlag Berlin Heidelberg 2006) ISBN-10 3-540-34709-7.

³ *Kondo effect of single Co adatoms on Cu surfaces*; N. Knorr, M. A. Schneider, L. Diekhöner, P. Wahl, and K. Kern, Phys. Rev. Lett. **88**, 096804 (2002).

⁴ *Interplay between structural, chemical, and spectroscopic properties of Ag/Au(111) epitaxial ultrathin films: A way to tune the Rashba coupling*; H. Cercellier, C. Didiot, Y. Fagot-Revurat, B. Kierren, L. Moreau, D. Malterre, and F. Reinert, Phys. Rev. B **73**, 195413 (2006).

⁵ *Surface-State Localization at Adatoms*; L. Limot, E. Pehlke, J. Kröger, and R. Berndt, Phys. Rev. Lett. **94**, 036805 (2005).

⁶ *Enhanced resolution imaging of ultrathin ZnO layers on Ag(111) by multiple hydrogen molecules in a scanning tun-*

neling microscope junction; S. Liu, A. Shiotari, D. Baugh, M. Wolf and T. Kumagai, Phys. Rev. B **97**, 195417 (2018).

⁷ *Surface-State Depopulation on Small Ag(111) Terraces*; Karina Morgenstern, Kai-Felix Braun, and Karl-Heinz Rieder, Phys. Rev. Lett. **89**, 226801 (2002).

⁸ *Depopulation of the Ag(111) Surface State Assigned to Strain in Epitaxial Films*; Georg Neuhold and Karsten Horn, Phys. Rev. Lett. **78**, 1327 (1997).

⁹ *Modifying the Cu (111) Shockley surface state by Au alloying*; Z. M. Abd El-Fattah, M. Matena, M. Corso, M. Ormaza, J. E. Ortega, and F. Schiller, Phys. Rev. B **86**, 245418 (2012); references therein.

¹⁰ *Piezoelectric-based apparatus for strain tuning*; C. W. Hicks, M. E. Barber, S. D. Eddins, D. O. Brodsky, and A. P. Mackenzie, Rev. Sci. Instrum. **85**, 65003 (2014).

¹¹ *Strong Increase of T_c of Sr_2RuO_4 Under Both Tensile and Compressive Strain*; C. W. Hicks, D. O. Brodsky, E. A. Yelland, A. S. Gibbs, J. A. N. Bruin, M. E. Barber, S. D. Eddins, K. Nishimura, S. Yonezawa, Y. Maeno, and A. P.

- Mackenzie, *Science* **344**, 283 (2014).
- ¹² *Kondo scattering observed at a single magnetic impurity*; J. Li, W.-D. Schneider, R. Berndt, and B. Delley, *Phys. Rev. Lett.* **80**, 2893 (1998)
 - ¹³ *Tunneling into a single magnetic atom: spectroscopic evidence of the Kondo resonance*; V. Madhavan, W. Chen, T. Jamneala, M. F. Crommie, and N. S. Wingreen, *Science* **280**, 567 (1998).
 - ¹⁴ *Quantum mirages formed by coherent projection of electronic structure*; H. C. Manoharan, C. P. Lutz, and D. M. Eigler, *Nature (London)* **403**, 512 (2000).
 - ¹⁵ *Enhanced hydrogen dissociation by individual Co atoms supported on Ag (111)*; D. Serrate, M. Moro-Lagares, M. Piantek, J. I. Pascual, and M. R. Ibarra, *J. Phys. Chem. C* **118**, 5827 (2014).
 - ¹⁶ *Quantifying the leading role of the surface state in the Kondo effect of Co/Ag(111)*, M. Moro-Lagares, J. Fernández, P. Roura-Bas, M.R. Ibarra, A. A. Aligia, and D. Serrate; *Phys. Rev. B.* **97** 235442 (2018).
 - ¹⁷ *Manipulation of the surface density of states of Ag(111) by means of resonators: Experiment and theory*; J. Fernández, María Moro-Lagares, D. Serrate and A. A. Aligia, *Phys. Rev. B* **94**, 075408 (2016).
 - ¹⁸ *Role of the surface state in the Kondo resonance width of a Co single adatom on Ag(111)*, Q. L. Li, C. Zheng, R. Wang, B. F. Miao, R. X. Cao, L. Sun, D. Wu, Y. Z. Wu, S. C. Li, B. G. Wang, and H. F. Ding; *Phys. Rev. B* **97**, 035417 (2018).
 - ¹⁹ *Single-molecule quantum dot as a Kondo simulator*; R. Hiraoka, E. Minamitani, R. Arafune, N. Tsukahara, S. Watanabe, M. Kawai, and N. Takagi, *Nat. Commun.* **8**, 16012 doi: 10.1038/ncomms16012 (2017).
 - ²⁰ *Symmetry-Driven Novel Kondo Effect in a Molecule*; E. Minamitani, N. Tsukahara, D. Matsunaka, Y. Kim, N. Takagi, and M. Kawai, *Phys. Rev. Lett.* **109**, 086602 (2012).
 - ²¹ *Theory of the Fano Resonance in the STM Tunneling Density of States due to a Single Kondo Impurity*; O. Újsághy, J. Kroha, L. Szunyogh, and A. Zawadowski, *Phys. Rev. Lett.* **85**, 2557 (2000).
 - ²² *Kondo temperature when the Fermi level is near a step in the conduction density of states*; J. Fernández, A. A. Aligia, P. Roura-Bas and J. A. Andrade *Phys. Rev. B* **95**, 045143 (2017).
 - ²³ R. Žitko, NRG LJUBLJANA , open source numerical renormalization group code, <http://nrgljubljana.ijs.si>
 - ²⁴ *Surface-State Lifetime Measured by Scanning Tunneling Spectroscopy*; J. Li, W.-D. Schneider, R. Berndt, O. R. Bryant and S. Crampin; *Phys. Rev. Lett.* **81**, 4464 (1998).
 - ²⁵ *Numerical renormalization group calculations of ground-state energy: Application to correlation effects in the adsorption of magnetic impurities on metal surfaces*; R. Žitko, *Phys. Rev. B* **79**, 233105 (2009).
 - son model*; H. O. Frota and L. N. Oliveira, *Phys. Rev. B* **33**, 7871 (1986); *Alternative discretization in the numerical renormalization-group method*; V. L. Campo and L. N. Oliveira, *Phys. Rev. B* **72**, 104432 (2005).
 - ²⁷ *Energy resolution and discretization artifacts in the numerical renormalization group*; R. Žitko and T. Pruschke, *Phys. Rev. B* **79**, 085106 (2009).
 - ²⁸ *Adaptive logarithmic discretization for numerical renormalization group methods*; R. Žitko, *Comput. Phys. Commun.* **180**, 1271 (2009).
 - ²⁹ *Mirages and many-body effects in quantum corrals*; A A Aligia and A M Lobos, *J. Phys.: Condens. Matter* **17** (2005) S1095S1122
 - ³⁰ A. C. Hewson, *The Kondo Problem to Heavy Fermions* (Cambridge University Press, Cambridge, England, 1997), ISBN 9780521599474.
 - ³¹ *A poor man's derivation of scaling laws for the Kondo problem*; P. W. Anderson, *J. Phys. C* **3**, 2436 (1970).
 - ³² *Review of techniques in the large-N expansion for dilute magnetic alloys*; N.E. Bickers, *Rev. of Mod. Phys.* **59**, 845 (1987).
 - ³³ *The renormalization group: Critical phenomena and the Kondo problem*; K. G. Wilson, *Rev. Mod. Phys.* **47**, 773 (1975).
 - ³⁴ *Numerical renormalization group method for quantum impurity systems*; Ralf Bulla, Theo A. Costi and Thomas Pruschke, *Rev. Mod. Phys.* **80**, 395 (2008).
 - ³⁵ *Kondo effect with a diverging hybridization: Possible realization in graphene with vacancies*; A. Mitchell and L. Fritz, *Phys. Rev. B* **88**, 075104 (2013).
 - ³⁶ *Impact of capacitance and tunneling asymmetries on Coulomb blockade edges and Kondo peaks in non-equilibrium transport through molecular quantum dots*; A. A. Aligia, P. Roura-Bas, and Serge Florens, *Phys. Rev. B* **92**, 035404 (2015).
 - ³⁷ *Width of the charge-transfer peak in the SU(N) impurity Anderson model and its relevance to non-equilibrium transport dot*; J. Fernández, F. Lisandrini, P. Roura-Bas, C. Gazza and A. A. Aligia, *Phys. Rev. B* **97**, 045144 (2018).
 - ³⁸ *Spectral density of an interacting dot coupled indirectly to conducting leads*; L. Vaugier, A.A. Aligia and A.M. Lobos, *Phys. Rev. B* **76**, 165112 (2007).
 - ³⁹ *Friedel sum rule for Anderson's model of localized impurity states*; D. C. Langreth, *Phys. Rev.* **150**, 516 (1966).
 - ⁴⁰ *Anderson model out of equilibrium: Noncrossing-approximation approach to transport through a quantum dot*, N. S. Wingreen and Y. Meir, *Phys. Rev. B* **49**, 11040 (1994).
 - ⁴¹ *Relation between width of zero-bias anomaly and Kondo temperature in transport measurements through correlated quantum dots: Effect of asymmetric coupling to the leads* D. Pérez Daroca, P. Roura-Bas, and A. A. Aligia, *Phys. Rev. B* **98** 245406 (2018).
 - ²⁶ *Photoemission spectroscopy for the spin-degenerate Ander-*